Clinical Biomechanics 54 (2018) 62–70

Contents lists available at ScienceDirect

Clinical Biomechanics

journal homepage: www.elsevier.com/locate/clinbiomech

# Patient-specific parameterised cam geometry in finite element models of femoroacetabular impingement of the hip

Robert J. Cooper*, Sophie Williams, Marlène Mengoni, Alison C. Jones

*Institute of Medical and Biological Engineering, School of Mechanical Engineering, University of Leeds, Leeds LS2 9JT, UK*

ARTICLE INFO

*Keywords:*
Femoroacetabular impingement
Finite element
Hip shape
Geometric parameterisation

ABSTRACT

*Background:* Impingement resulting in soft tissue damage has been observed in hips with abnormal morphologies. Geometric parameterisation can be used to automatically generate a range of bone geometries for use in computational models, including femurs with cam deformity on the femoral neck.

*Methods:* This study verified patient-specific parametric finite element models of 20 patients with cam deformity (10 female, 10 male) through comparison to their patient-specific segmentation-based equivalents. The parameterisation system was then used to generate further models with parametrically defined geometry to investigate morphological changes in both the femur and acetabulum and their effects on impingement.

*Findings:* Similar findings were observed between segmentation-based and parametric models when assessing soft tissue strains under impingement conditions, resulting from high flexion and internal rotations. Parametric models with cam morphology demonstrated that clinically used alpha angles should not be relied on for estimating impingement severity since planar views do not capture the full three-dimensional geometry of the joint. Furthermore, the parametric approach allowed study of labral shape changes, indicating higher strains can result from bony overcoverage.

*Interpretation:* The position of cams, as well as their size, can affect the level of soft tissue strain occurring in the hip. This highlights the importance of reporting the full details of three-dimensional geometry used when developing computational models of the hip joint and suggests that it could be beneficial to stratify the patient population when considering treatment options, since certain morphologies may be at greater risk of elevated soft tissue strain.

## 1. Introduction

Abnormal bone morphology in the hip is associated with femoroacetabular impingement (FAI), in which repeated contact between the proximal femur and the acetabular rim can result in pain and intra-articular damage (Ganz et al., 2003). A particular example is cam deformity, in which excess bone is present on the femoral neck. Cams most typically occur in young adults, and are more prevalent among males (Kuhns et al., 2015). Understanding of the circumstances leading to symptomatic impingement remains elusive, especially because some hips possessing morphology characteristic of FAI remain asymptomatic (Khanna et al., 2014).

In order to investigate the effects of bone morphology on tissue strains computationally, it is useful to be able to automatically generate multiple geometries representative of the population variation. This can be achieved using a parametric approach to finite element models of the hip (Hua et al., 2015; Chegini et al., 2009). A recent study (Hua et al., 2015) demonstrated that parameterised models could identify differences in contact mechanics between two different subjects with healthy hips across a gait cycle, providing confidence that such models can be used to systematically evaluate the effects of clinically relevant changes in morphology. However, some studies suggest that models with idealised geometry can lead to poor estimates of hip contact stresses (Gu et al., 2011; Anderson et al., 2010). It is therefore important that parametric models are compared with segmented patient-specific models in order to understand the effects of smoothing out local undulations in subject-specific articular geometries. As well as isolating the effects of individual changes, parametric models with simplified articular surfaces can alleviate computational convergence issues (Hellwig et al., 2016) reported to occur when using more complex geometry (Jorge et al., 2014).

Geometrical variations generated in parametric models must be well defined. Clinically used radiographic measurements such as the alpha angle, which estimates the asphericity of the femoral head, are highly dependent on the two-dimensional radiographic view of the joint and do not capture the full three-dimensional geometry (Cooper et al.,

* Corresponding author.
*E-mail address:* r.j.cooper@leeds.ac.uk (R.J. Cooper).

https://doi.org/10.1016/j.clinbiomech.2018.03.007
Received 27 October 2017; Accepted 13 March 2018

2017; Harris et al., 2014). Alpha angles can therefore be ambiguous and are not well suited to describing geometrical variation.

Contact pressures and stresses have been widely used to assess cartilage compression and potential degradation (Gu et al., 2011; Anderson et al., 2010; Jorge et al., 2014; Ng et al., 2016), but strains and positional changes in soft tissues, especially the labrum and cartilage-labrum junction, may be more pertinent for improving understanding of when impingement damage may occur. Abutment of the cam against the acetabular rim may result in damage due to cartilage abrasion and translation of the labrum away from the joint (Kuhns et al., 2015; Banerjee & Mclean, 2011).

The aims of this study were to:

1) Establish the effect of geometric simplification in finite element models of impingement when assessing labrum displacement and cartilage-labrum junction strain.
2) Demonstrate the capability of the parameterisation system in distinguishing the effects of cam size and position, beyond what is possible using an alpha angle measurement.
3) Assess the effects of parametrically varying labrum size and labrum-bone ratio.

## 2. Methods

We previously developed a geometric parameterisation system capable of representing segmented femurs with cam deformity with root mean squared surface fitting errors in the region of 0.6 mm, allowing isolation of the size and position of cams (Cooper et al., 2017). The parameterisation method allowed generation of new femoral geometries with the neck region described by ellipses (Fig. 1).

### 2.1. Segmented vs parametric femoral geometry

Femurs from 10 female and 10 male patients (age range 22–49 years, median 34.5), with clinically diagnosed cam deformity were segmented from CT images (Sensation 16 CT scanner, Siemens, Berlin and Munich, Germany, voxel size: 0.7422 × 0.7422 × 1 mm) using Simpleware ScanIP 7.0 (Synopsys, Mountain View, USA). Ethical approval was granted by the University of Leeds MEEC research ethics committee (MEEC 11-044). A parameterisation method (Cooper et al., 2017) was used to generate an equivalent parametric model for each segmented model (Fig. 2).

Simplified geometry representing the acetabulum was created as a spherical cup shape with 33% of the surface area of a complete sphere. Spherical acetabular cartilage was included with the acetabular fossa represented by removing a notch from the centre region. The labrum was generated by sweeping a triangular cross section (Chegini et al., 2009; Banerjee & Mclean, 2011) about the circular acetabular rim. This basic acetabular geometry was scaled according to the head radius of each femur to provide a mean cartilage thickness of approximately 1 mm across all models. Let HR denote the femoral head radius of a given model, then the acetabular cartilage thickness was assigned as HR/A where A = 22.95 mm, based on the average head radius for the 20 hips. The labrum length was 7HR/25 mm (Chegini et al., 2009). In all models, the acetabulum was rotated to simulate a standardised anteversion angle of 20° and centre edge angle of 30°. These angles were chosen based on reported average values for CE and AV angles, including the subjects in this study (Chegini et al., 2009; Cooper et al., 2017; Ergen et al., 2014; Tannast et al., 2007).

Starting from a 90° flexion position, boundary conditions were used to simulate internal rotation of the femurs up to a maximum of 35°. In all cases, the acetabulum was fixed in place whilst the femur was constrained in translation and rotated to impinge against the labrum. Contact between surfaces was modelled as frictionless with finite sliding and hard contact (linear penalty algorithm). Femurs were by default rotated about their head centre, but in practice this was only successful in six cases. In the other cases, this rotation either caused severe overclosure of the femoral and acetabular surfaces, or did not result in the cam contacting the labrum. In each case the point of rotation was adjusted on the femoral neck axis to optimise for convergence whilst achieving impingement against the labrum without overclosure due to the irregular contact surfaces. The same boundary conditions were used for the segmented and parametric models of each individual patient.

Generation of all models was automated in Abaqus 6.14 (Dassault Systèmes, Vélizy-Villacoublay, France) using Python. All FE models were quasi-static analyses, with geometric non-linearity.

### 2.2. Parametric morphology tests

In order to demonstrate the capability of the parameterisation system, it was used to generate additional parametric models. Boundary conditions in these models simulated flexion from 70° to 90°, followed by up to 35° of internal rotation.

Four models were created with parametrically varied femurs. Maintaining a constant head radius of 25 mm, parameters defining the neck region were adjusted to define four variations, featuring two different cam radii (low and high) and two cam positions (anterior and superior). Alpha angles of these four parametric femurs were measured as the angle between the line passing through the femoral neck midpoint and the femoral head centre, and the line from the femoral head centre to the anterior point where the femoral head diverges from spherical. This was done in anterior-posterior (AP) and in cross-table lateral views using ImageJ 1.51 k (National Institute of Health, Rockville, USA) (Schindelin et al., 2012).

A further five models were generated in which the acetabulum was

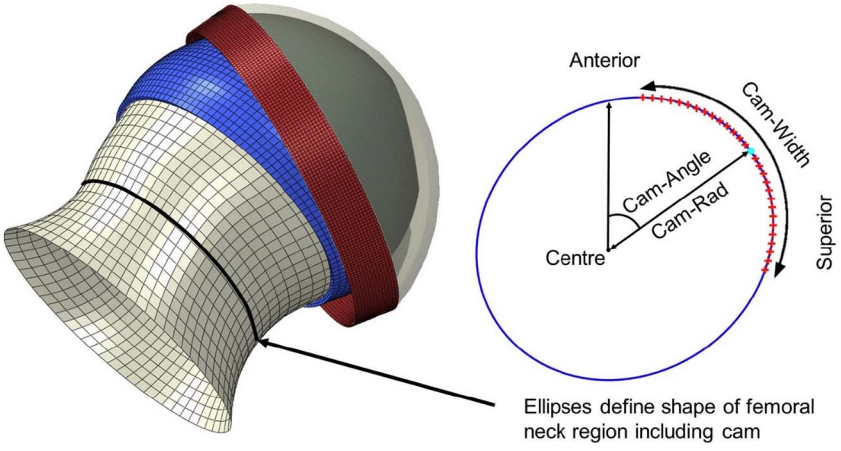


**Fig. 1.** Five ellipses fitted to cross sections of the femoral neck at automatically defined positions, along with a spherical cap, generated the parametric femoral geometry. The first four ellipses were linearly spaced between x/2 and x, where x is the total number of slices (rounding these points to integer values). A 5th ellipse was at HR × 1.2. Cam size and position was determined by measurements on the 2nd and 3rd ellipses, focusing on the cam region. Cam angle indicates the position of the cam, whilst radius and width together indicate the cam extent (Cooper et al., 2017).

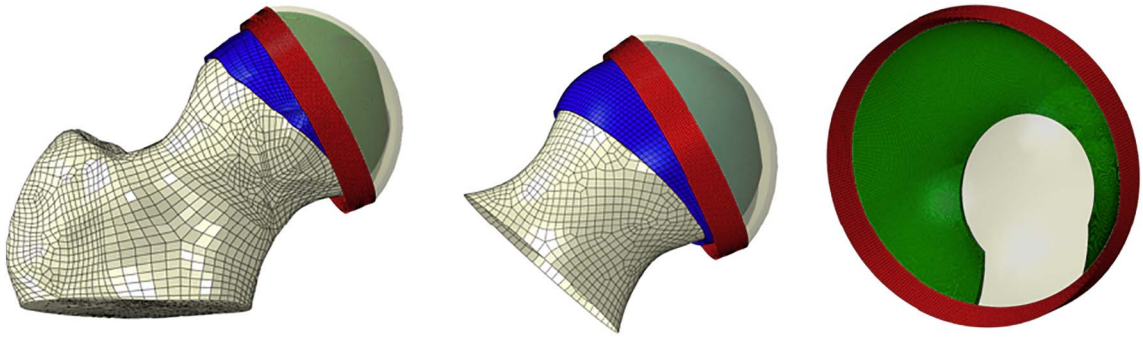

**Fig. 2.** Examples of meshed models showing segmented and parameterised femurs, and the acetabulum, modelled as rigid surfaces. Femoral cartilage elements are blue, acetabular labrum elements are red, and acetabular cartilage elements are green. (For interpretation of the references to colour in this figure legend, the reader is referred to the web version of this article.)

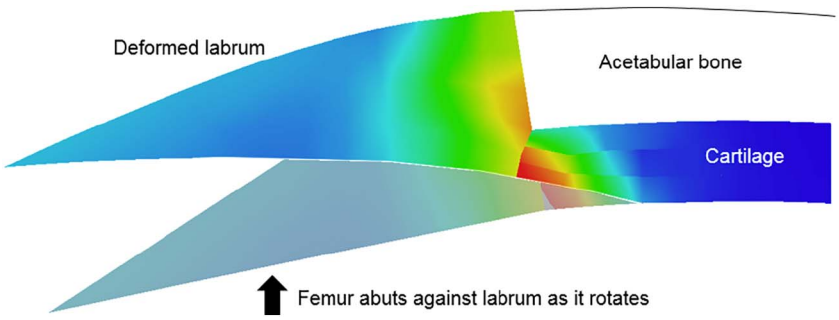


**Fig. 3.** Example of a cross-section through a deformed (bright colour) and undeformed (shaded) cartilage-labrum junction. Regions of high tensile strain are displayed in red. (For interpretation of the references to colour in this figure legend, the reader is referred to the web version of this article.)

parametrically varied. In these cases the femur was assigned a constant cam radius and position. The base model used the same acetabulum used in the previous models. The four additional cases were: increased labrum length, with unchanged and increased overall coverage; and decreased labrum length, with unchanged and decreased overall coverage.

### 2.3. Outputs of interest

Peak displacements in the labrum and tensile strains (maximum principal logarithmic strain) at the cartilage-labrum junction were recorded throughout the simulations. Maximum displacements occurred at the labral tip and this gave one indication in each case of the severity of impingement as the labrum was deformed by the cam. Tensile strain occurring at the cartilage-labrum junction area was also of interest because this deformation may be a cause of cartilage surface fibre damage. To quantify model agreement, the difference in results between parametric and segmented models was recorded after every 5° of rotation, allowing the root mean squared difference for each specimen to be calculated.

### 2.4. Material properties

In all models in this study, femoral bones and the acetabulum were modelled as rigid bodies (Chegini et al., 2009; Anderson et al., 2008). Femoral cartilage was assigned with isotropic linearly elastic material properties ($E = 12$ MPa, $\nu = 0.4$) (Chegini et al., 2009; Jorge et al., 2014). Biphasic cartilage properties were not considered in this study since modelling cartilage as elastic is an appropriate simplification to predict short term contact stresses (Henak et al., 2013; Ateshian et al., 2007).

Acetabular cartilage and the labrum were also modelled as linearly elastic, but were assigned transversely isotropic properties defined according to typical collagen fibril alignment. Collagen fibrils in cartilage are believed to be orientated parallel to the articular surface in outer layers, but perpendicular and anchored to the bone in inner layers (Sophia Fox et al., 2009; Meng et al., 2017; Osawa et al., 2014). Thus the elastic modulus in the direction perpendicular to the articular surface was assigned to be greatest at the base layer (boundary between subchondral bone and cartilage), reduced in the middle layer and lowest at the articular surface. The modulus in the directions perpendicular to the articular surface was assigned to be greatest at the surface, reduced in the middle layer and lowest at the base layer ($E = 9$, 12, 15 MPa respectively). Collagen fibrils in the labrum are believed to be predominantly aligned circumferentially (Petersen et al., 2003; Grant et al., 2012), so a greater modulus was assigned in the circumferential direction ($E = 20$ MPa and 12 MPa respectively). In all acetabular cartilage layers and in the labrum, Poisson's ratio was set as $\nu = 0.4$ and the shear modulus $G$ was assigned so that $2G = (E_{mean}) / (1 + \nu)$.

### 2.5. Mesh generation and sensitivity

Hexahedral meshes were desired for meshing soft tissues because linear tetrahedral elements are stiffer than hexahedral elements, and using tetrahedral elements for contact problems can result in locking, large stress concentrations and poor estimations of contact areas (Maas et al., 2016). Quadrilateral meshes were therefore required on bone surfaces. To achieve quadrilateral meshes on segmented bone surfaces, they were exported from ScanIP using the +NURBS module and subsequently meshed within Abaqus. Femoral cartilage layers were produced as orphan hexahedral meshes created by offsetting the meshes on the femoral bone parts (thickness 1 mm). Acetabular cartilage and the labrum were also meshed with hexahedral elements.

The mesh density adopted was determined after mesh convergence tests. Displacements seen in the models were converged at the mesh density of three elements across the thickness of the acetabular cartilage and labrum, but local strain was more sensitive to mesh resolution.

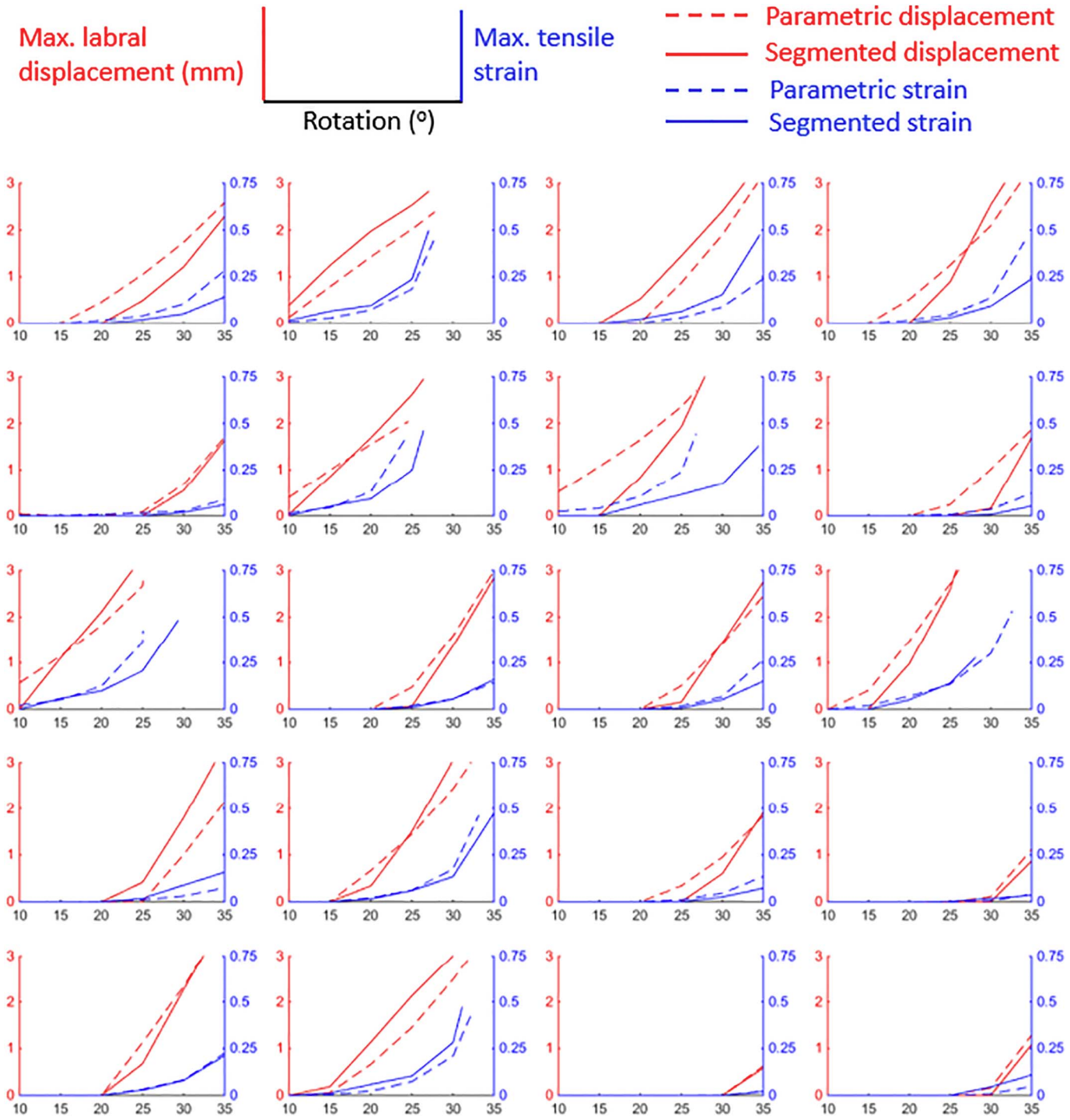


**Fig. 4.** Graphs comparing segmented (solid lines) and parametric (dashed lines) models for each of the 20 cam patients, showing maximum labral displacement (blue, left y-axes, in mm) and cartilage-labrum junction strain (red, right y-axes as maximum principal logarithmic strains) with increasing internal rotation of the femur (x-axes, in degrees). (For interpretation of the references to colour in this figure legend, the reader is referred to the web version of this article.)

To achieve convergence for all outputs of interest, six elements were used across the thickness of the acetabular cartilage and labrum (that is, two elements for each distinct cartilage layer), resulting in approximately 156,000 elements for the acetabular soft tissue (8-node linear brick, reduced integration, enhanced hourglass control). Only two elements were used across the thickness of the femoral cartilage because outputs from acetabular side were of interest and the femoral cartilage did not affect contact between the bony cam and acetabular-labral junction.

## 3. Results

The data associated with this paper are openly available from the University of Leeds data Repository (Cooper et al., 2018).

For the segmented and equivalent parametric models, the range of positions used for the centre of rotation was −2 mm to 4 mm (where positive is more proximal), and the average position was 1.2 mm proximally above the femoral head centre. The level of internal rotation achieved ranged from 23° to 35°. In all models the typical deformation pattern consisted of displacement of the labrum and compression of the

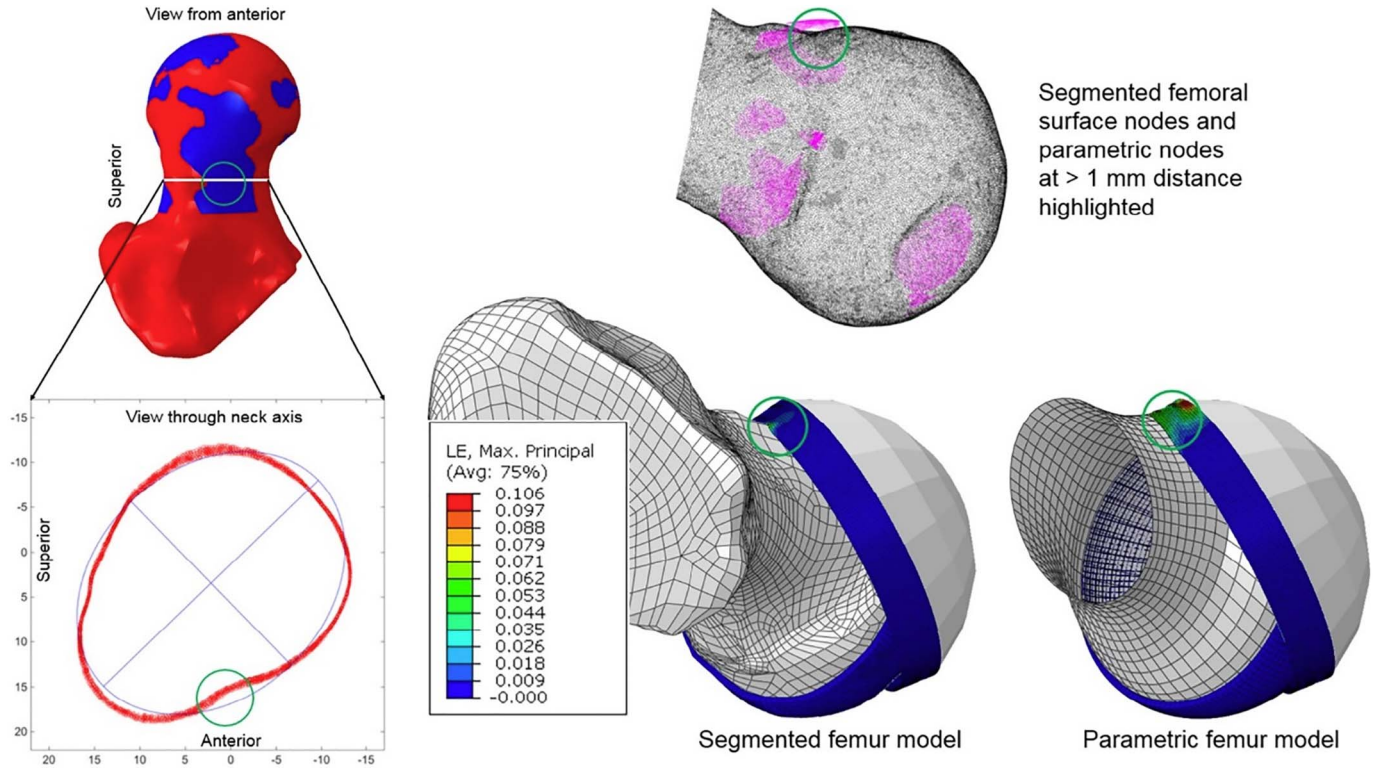


**Fig. 5.** Illustration of differences between segmented (red) and parametric (blue) models due to poor local fit. Poor local fit is a result of the best fit ellipse failing to adequately capture the shape of vertices from a slice of the segmented femoral neck. Parametric model nodes (pink) at a distance > 1 mm from the nearest segmented model node (black) highlight an example of poor local fit, leading to higher labral strain and displacement (shown at 20° internal rotation). (For interpretation of the references to colour in this figure legend, the reader is referred to the web version of this article.)

cartilage-labrum junction (Fig. 3). Generally similar displacements and strains occurred in the segmented and equivalent parametric models; the range in root mean squared difference in results for the segmented and parametric models was 0.0039–0.1292 mm for peak labral displacement and 0.0002–0.0134 for peak strain (Fig. 4). For context, displacements peaked at 5.4 mm, and strains peaked at 0.53. The lower levels of agreement occurred when the local fitting errors between the parametric and segmented surfaces in the cam region were larger, particularly > 1 mm. (Fig. 5).

High deformation of elements in the cartilage-labrum junction prevented models converging past a certain level of rotation, so for the additional parametric tests, rotation levels where all models converged were used to generate comparison graphs. This was 15° for the models where cam morphology was varied (Fig. 6) and 25° for the models where acetabular rim morphology was varied (Fig. 7).

When cam morphology was varied, measured alpha angles did not predict outputs of interest (Fig. 6). In particular, AP alpha angles were unexpectedly higher ($\alpha = 63.4°$, $\alpha = 83.1°$) in the cases with no labral displacement occurring at 15° rotation than in cases where labral displacement did occur ($\alpha = 41.5°$, $\alpha = 44.6°$). The cross-table lateral alpha angle was largest ($\alpha = 83.2°$) in the most severe impingement case (peak strain = 0.3793), but did not distinguish between the other models ($\alpha$ range = 61.0°–68.5°) where impingement severity varied as a result of cam size and position as defined on the neck ellipses (strain range = 0.0283–0.0341, displacement range = 0–1.52 mm).

When acetabular rim and labral morphology was varied, an increase to bone coverage had the greatest effect on impingement severity (Fig. 7). A 10% increase in bone (with labrum size decreased to maintain the same overall coverage) increased strain in the cartilage labral-junction from 0.1155 to 0.4053. Increasing labral length by 10% (thus increasing overall coverage) increased labral displacement from 2.76 mm to 3.29 mm, but had little effect on junction strain, which increased from 0.1155 to 0.1253.

## 4. Discussion

The aims of this study were to validate the use of geometrically parameterised femoral surfaces against segmented equivalents, and to use parametric models to assess key hip shape morphological variations in 3D. Subject-specific parametric models were compared with segmented models and trends in parametric models were found to be largely in agreement with segmented models. Additionally generated parametrically defined femurs demonstrated the issues with relying on 2D alpha angle measures as an indication of impingement severity potential. A simplified labrum geometry allowed rapid investigation of the effects of morphological variations and suggested bony overcoverage can increase impingement severity. High strains at the cartilage-labral junction resulting from direct compression of the cartilage by the cam, rather than the stretching of cartilage as a result of displacement of the labrum, were seen to be the driver of elevated tensile strains in cartilage in the models.

### 4.1. Segmented vs parametric models

Similar displacements and strains occurred in the segmented and equivalent parametric models. This suggested that these outputs were relatively insensitive to the local undulations on the articular surface, which were present in the segmented models but smoothed out in the parametric representation. Previous modelling studies have reported elevated contact pressures and stresses in the anterosuperior cartilage and labrum (Chegini et al., 2009; Jorge et al., 2014; Ng et al., 2016), matching clinical reports of damage (Beck et al., 2005). This corroborates with findings of high strain in the cartilage-labral junction in the models developed in this study.

The comparison between segmented and parametric models provided confidence in the results, in that trends and magnitudes present in segmented models were replicated in parametric models. There was no

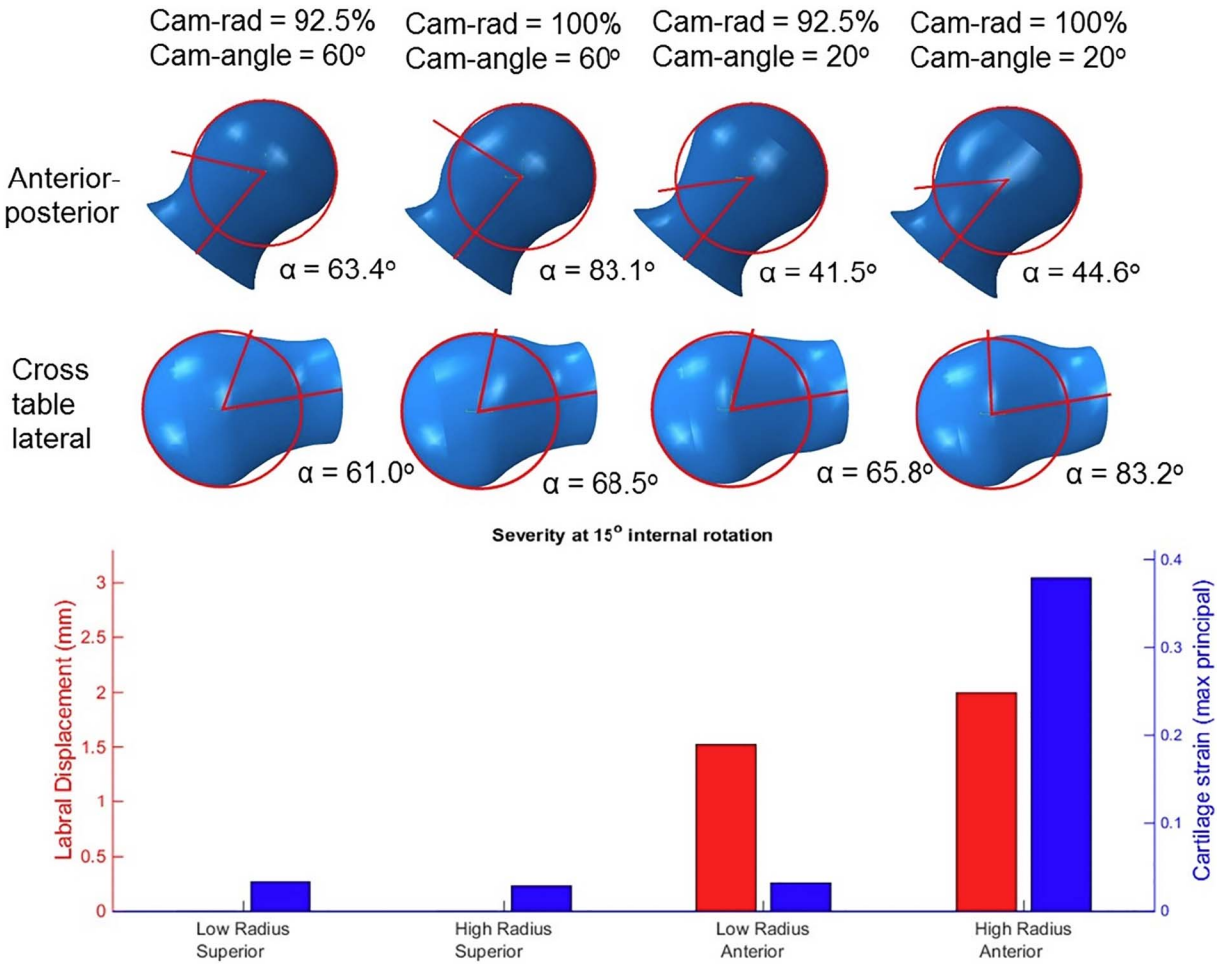


**Fig. 6.** Labral displacement and cartilage strain for 4 femoral parametric models at 15° internal rotation and full flexion, with indication of clinical alpha angles. Alpha angles showed poor correlation to results from parametric models.

direct validation since there were other simplifications to the models in terms of boundary conditions and material properties. Measurement of impingement risks by the outcome of the FE models should therefore not be understood as absolute risk. Other studies comparing segmented and parameterised models suggested idealised geometry can underestimate contact stresses occurring in the hip (Gu et al., 2011; Anderson et al., 2010), but did not specifically investigate geometry related to impingement. In the impingement scenario modelled here, it was possible to identify the underlying cause of differences in model outputs by quantifying poor fitting between the smooth, parametric surfaces and more undulating, segmented surfaces in contact regions.

Given the chosen boundary conditions, displacement of the labrum is a result of the position and peak size of the cam. When a poorer fit between the parametric and segmented surfaces at the cam region occurred, impingement contact arose at appreciably smaller rotation angles in the parametric or segmented case, depending on whether the parametric surface over- or under-estimated the radius of the segmented cam. Earlier contact in the model with the larger radius resulted in more displacement of the acetabular soft tissue at lower angles of rotation. When higher labral displacement occurred in the segmented or parametric model, the tensile strain in the cartilage-labrum junction was usually also higher, since the cartilage was both more compressed by the cam and stretched more as a result of the labral displacement. However discrepancies in the local fit between surfaces at the cam region could be such that the labral tip displacement was higher, whilst the cartilage was compressed less and had lower tensile strain. This emphasises that although a low overall geometrical fitting error can be achieved (Cooper et al., 2017), it does not guarantee that the parametric geometry is able to precisely capture the shape of all cams. The fit in localised regions may be poorer than the overall fit, which in the impingement scenario is of particular importance in the cam region (Fig. 5).

### 4.2. Parametric tests

Models incorporating parametric femoral variations revealed that cams positioned more anteriorly resulted in more severe impingement in the simulated scenario (flexion followed by internal rotation) (Fig. 6). However, the AP alpha angle on both the anterior cam models was lower than those on the superior cam models. AP alpha angles gave the opposite prediction to the severity indicated by the model outputs, because superior cams were more visible in the AP view. In the anterior cam models, the AP alpha angle increased by only 3.3° when the cam radius was increased, but the severity in the model increased dramatically, indicated by an increase in tensile strain in the cartilage-labrum junction from 0.03 to 0.38. For superior cams, increasing the cam radius substantially increased the AP alpha angle, but the additional severity observed in the model was less than that seen between the anterior cam models. Thus using an AP alpha angle, it was not possible to predict the severity of impingement.

Alpha angles above 55° have been suggested as indicators of cam impingement (Tannast et al., 2007; Urquhart et al., 2014; Pfirrmann et al., 2006), so the alpha angles generated here were clinically relevant. The cross-table lateral alpha angle was largest in the most severe impingement case (83.2°), but did not however distinguish between the other models, with similar angles (all above 60°, with a range of 7.5°)

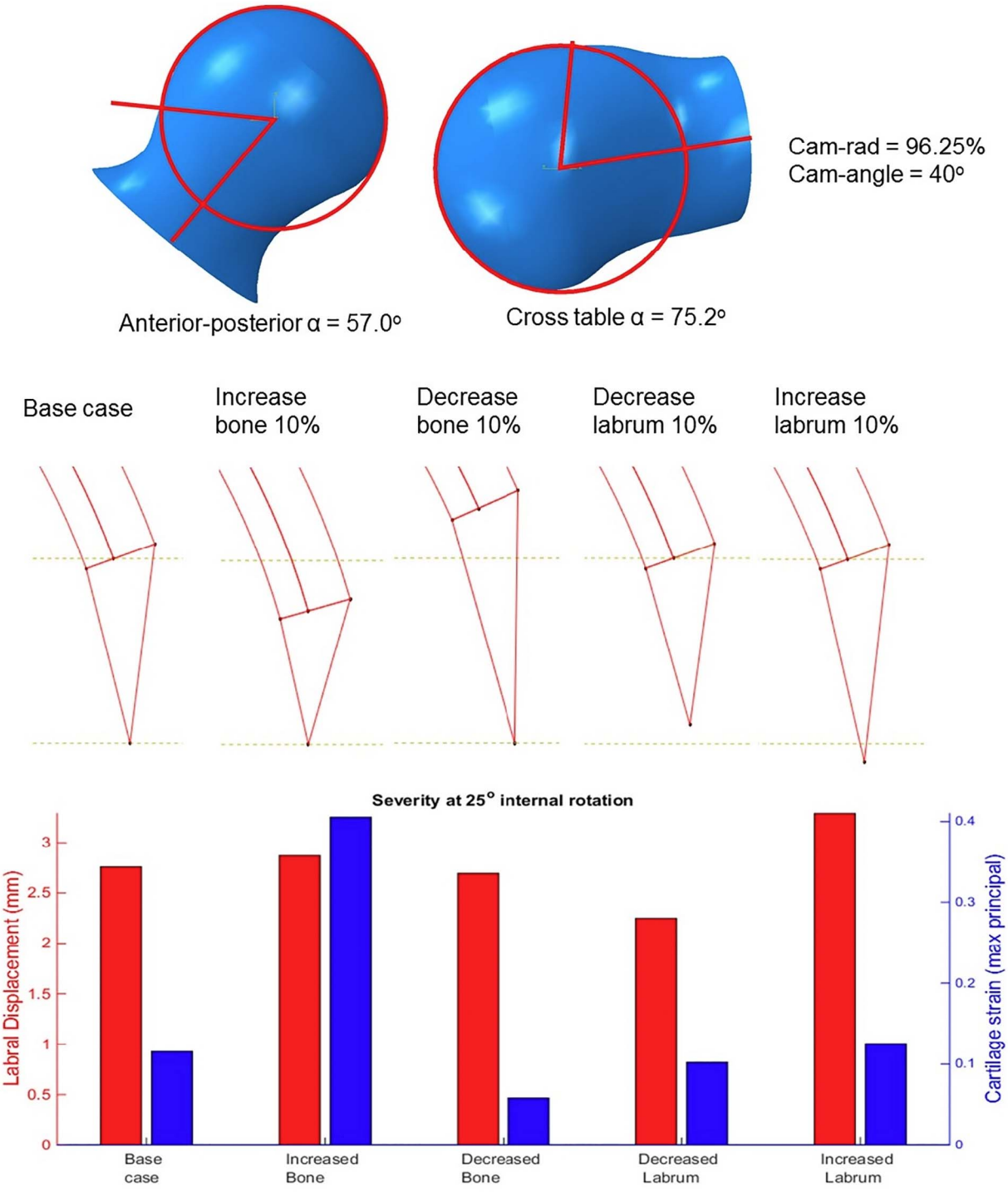


**Fig. 7.** Labral displacement and cartilage strain for 5 acetabular parametric models at 25° internal rotation and full flexion, with indication of clinical alpha angles. Strain increased with greater bone coverage.

recorded for the three models. The differences in severity predicted by the models were a result of both the extent and the position of the cams defined in 3D measurements.

In the acetabular coverage tests, greater bony coverage resulted in increased strain (Fig. 7). The models therefore predicted that elevated bony acetabular coverage likely increases impingement severity for a given level of rotation. Labral displacement appeared to be driven by the position of its tip relative to the cam, rather than overall labral length. The model with increased labrum length but the same overall coverage (less bone), exhibited less strain at the junction, because the bulk of the labrum was located further from the labral tip when impingement was initiated. It has been suggested that in dysplastic hips, labral length may be increased in the weight-bearing zone, potentially compensating for the lack of bony coverage (Garabekyan et al., 2016). The results reported here suggest that the increase in coverage caused by this reaction may not increase impingement severity to the same extent as in cases where coverage is elevated due to excess acetabular bone.

### 4.3. Limitations and challenges

The models in this study suggest direct compression of the cartilage

by the cam as the main cause of impingement damage, but it is important to consider limitations which could mean that effect of labral displacement is underemphasised. Soft tissues were not visible in the patient CT scans and as such, femoral cartilage geometry was estimated by expanding the geometry of the bone, providing consistent methodology for parametric and segmented surfaces. In addition, the current method of generating parametric models requires bone segmentation from 3D images. There are clear benefits to being able to take detailed bone measurements from lower radiation dose imaging systems (Thelen et al., 2017). However, any reduction in image resolution and associated increase in distance between image slices, reduces the precision by which we can establish the cam size and location.

Simplified acetabular geometry was chosen for all models in order to facilitate parametric assessment of labral changes, and to mitigate convergence issues that resulted from contact between irregular articular surfaces. It is important to appreciate that significant subject-specific differences also occur on the acetabular side, which could result in altered tissue strains, since the fit of the femoral head into the acetabulum may vary between patients. Parametric study of geometrical changes to the femur here assumed constant acetabular geometry. Whilst parametric study of changes to the labrum was also conducted, the labrum was defined on a circular acetabular rim, and not verified against subject-specific cases as the femurs were. This was because labral tissue could not be segmented from the clinical CT scans. Furthermore, specimen-specific values for acetabular angles were not deemed appropriate for comparing parametric and segmented models, since it was important to ensure a certain degree of impingement occurred in order to compare trends seen in parametric and segmented cases, and the simplification to spherical acetabular geometry meant that adjusting acetabular angles would unnecessarily restrict the possible range of movement that could be simulated.

The adopted approach modelled impingement using applied internal rotations from a flexion position. Previously published loading data (Bergmann et al., 2001) was deemed inappropriate since FAI patients are younger and have deformities that could result in altered gait patterns. In the segmentation/parametric comparison models, it was important to ensure the same boundary conditions were applied to both models of each individual patient. Femurs were generally rotated about their head centre; in some cases this caused excessive penetration of the femoral and acetabular surfaces, preventing convergence. Therefore the point of rotation was adjusted to optimise for model convergence whilst achieving impingement against the labrum. To ensure a valid comparison, the boundary conditions were always consistent for the parametric and segmented models of each patient. Differences between boundary conditions used for distinct patients however meant that models of different patients were not directly comparable. The use of parametric models (without the restriction of requiring boundary conditions to match a segmented case) mitigates this problem because the smoother surfaces are less prone to these errors. Additional parametric models varying the femur and acetabulum could therefore be developed and were used to assess the effects of individual morphological variations. Even so, high deformation of elements in the cartilage-labrum junction prevents models converging past a certain level of rotation, so results from lower rotation levels were required to compare models exhibiting severe impingement.

### 4.4. Conclusions

This study has quantified the effects of using parametric geometries when investigating femoroacetabular impingement, by comparison with a gold standard segmentation approach. In a simulation of the impingement scenario, we showed that discrepancies resulted from possible poor local fit in the cam region, but trends in outcomes of interest were similar between modelling methods. Whilst still requiring full 3D segmentation, there is potential to further develop parametric methods to assess impingement severity based only on measures of the neck and acetabulum.

The parametric study demonstrated the enhanced capability of a three-dimensional analysis over current clinical measures of planar alpha angles, which are highly dependent on view. Potential for tissue damage was not predicted by alpha angle measures. We previously reported that among the 20 patients included in this study, females were more likely to have cams located in an anterior position, which are less visible in AP radiographs (Cooper et al., 2017). In the impingement scenarios tested here, anterior cams caused greater levels of soft tissue strain and could therefore result in more severe articular damage. Although cams are more common in males and tend to be more diffuse in females, their position in females could make them more severe.

## Acknowledgements

This work was funded by the EPSRC (grant number EP/F500513/1) and the ERC (grant number StG-2012-306615). Models were run using the University of Leeds high performance computing cluster ARC2.

## References

Anderson, A.E., Ellis, B.J., Maas, S.A., Peters, C.L., Weiss, J.A., 2008. Validation of finite element predictions of cartilage contact pressure in the human hip joint. J. Biomech. Eng. 130 (5), 051008. http://dx.doi.org/10.1115/1.2953472.

Anderson, A.E., Ellis, B.J., Maas, S.A., Weiss, J.A., 2010. Effects of idealized joint geometry on finite element predictions of cartilage contact stresses in the hip. J. Biomech. 43 (7), 1351–1357. http://dx.doi.org/10.1016/j.jbiomech.2010.01.010.

Ateshian, G.A., Ellis, B.J., Weiss, J.A., 2007. Equivalence between short-time biphasic and incompressible elastic material responses. J. Biomech. Eng. 129 (3), 405–412. http://dx.doi.org/10.1115/1.2720918.

Banerjee, P., Mclean, C.R., 2011. Femoroacetabular impingement: a review of diagnosis and management. Curr. Rev. Muscoskelet. Med. 4 (1), 23–32. http://dx.doi.org/10.1007/s12178-011-9073-z.

Beck, M., Kalhor, M., Leunig, M., Ganz, R., 2005. Hip morphology influences the pattern of damage to the acetabular cartilage. J. Bone Joint Surg. 87 (7), 012–1018. http://dx.doi.org/10.1302/0301-620X.87B7.15203.

Bergmann, G., Deuretzbacher, G., Heller, M., Graichen, F., Rohlmann, A., Strauss, J., Duda, G.N., 2001. Hip contact forces and gait patterns from routine activities. J. Biomech. 34 (7), 859–871. http://dx.doi.org/10.1016/S0021-9290(01)00040-9.

Chegini, S., Beck, M., Ferguson, S.J., 2009. The effects of impingement and dysplasia on stress distributions in the hip joint during sitting and walking: a finite element analysis. J. Orthop. Res. 27 (2), 195–201. http://dx.doi.org/10.1002/jor.20747.

Cooper, R.J., Mengoni, M., Groves, D., Williams, S., Bankes, M.J.K., Robinson, P., Jones, A.C., 2017. Three-dimensional assessment of impingement risk in geometrically parameterised patient hips compared with clinical measures. Int. J. Numer. Methods Biomed. Eng. 33 (11), e2867. http://dx.doi.org/10.1002/cnm.2867.

Cooper, R.J., Williams, S., Mengoni, M., Jones, A.C., 2018. Dataset Associated with 'Patient-Specific Parameterised Cam Geometry in Finite Element Models of Femoroacetabular Impingement in the Hip'. University of Leeds, UK. https://doi.org/10.5518/326.

Ergen, F.B., Vudali, S., Sanverdi, E., Dolgun, A., Aydingöz, Ü., 2014. CT assessment of asymptomatic hip joints for the background of femoroacetabular impingement morphology. Diagn. Interv. Radiol. 20 (3), 271. http://dx.doi.org/10.5152/dir.2013.13374.

Ganz, R., Parvizi, J., Beck, M., Leunig, M., Nötzli, H., Siebenrock, K.A., 2003. Femoroacetabular impingement: a cause for osteoarthritis of the hip. Clin. Orthop. Relat. Res. 417, 112–120. http://dx.doi.org/10.1097/01.blo.0000096804.78689.c2.

Garabekyan, T., Ashwell, Z., Chadayammuri, V., Jesse, M.K., Pascual-Garrido, C., Petersen, B., Mei-Dan, O., 2016. Lateral acetabular coverage predicts the size of the hip labrum. Am. J. Sports Med. 44 (6), 1582–1589. http://dx.doi.org/10.1177/0363546516634058.

Grant, A.D., Sala, D.A., Davidovitch, R.I., 2012. The labrum: structure, function, and injury with femoroacetabular impingement. J. Child. Orthop. 6 (5), 357–372. http://dx.doi.org/10.1007/s11832-012-0431-1.

Gu, D.Y., Hu, F., Wei, J.H., Dai, K.R., Chen, Y.Z., 2011. Contributions of non-spherical hip joint cartilage surface to hip joint contact stress. In: Engineering in Medicine and Biology Society. EMBC, Annual International Conference of the IEEE, pp. 8166–8169.

Harris, M.D., Kapron, A.L., Peters, C.L., Anderson, A.E., 2014. Correlations between the alpha angle and femoral head asphericity: implications and recommendations for the diagnosis of cam femoroacetabular impingement. Eur. J. Radiol. 83 (5), 788–796. http://dx.doi.org/10.1016/j.ejrad.2014.02.005.

Hellwig, F.L., Tong, J., Hussell, J.G., 2016. Hip joint degeneration due to cam impingement: a finite element analysis. Comput. Methods Biomech. Biomed. Engin. 19 (1), 41–48. http://dx.doi.org/10.1080/10255842.2014.983490.

Henak, C.R., Anderson, A.E., Weiss, J.A., 2013. Subject-specific analysis of joint contact mechanics: application to the study of osteoarthritis and surgical planning. J. Biomech. Eng. 135 (2), 021003. http://dx.doi.org/10.1115/1.4023386.

Hua, X., Li, J., Wilcox, R.K., Fisher, J., Jones, A.C., 2015. Geometric parameterisation of

pelvic bone and cartilage in contact analysis of the natural hip: an initial study. Proc. Inst. Mech. Eng. H J. Eng. Med. 229 (8), 570–580. http://dx.doi.org/10.1016/j.medengphy.2004.12.008.

Jorge, J.P., Simões, F.M., Pires, E.B., Rego, P.A., Tavares, D.G., Lopes, D.S., Gaspar, A., 2014. Finite element simulations of a hip joint with femoroacetabular impingement. Comput. Methods Biomech. Biomed. Engin. 17 (11), 1275–1284. http://dx.doi.org/10.1080/10255842.2012.744398.

Khanna, V., Caragianis, A., DiPrimio, G., Rakhra, K., Beaulé, P.E., 2014. Incidence of hip pain in a prospective cohort of asymptomatic volunteers is the cam deformity a risk factor for hip pain? Am. J. Sports Med. 42 (4), 793–797. http://dx.doi.org/10.1177/0363546513518417.

Kuhns, B.D., Weber, A.E., Levy, D.M., Wuerz, T.H., 2015. The natural history of femoroacetabular impingement. Frontiers in surgery. 2, 58. http://dx.doi.org/10.3389/fsurg.2015.00058.

Maas, S.A., Ellis, B.J., Rawlins, D.S., Weiss, J.A., 2016 Mar 21. Finite element simulation of articular contact mechanics with quadratic tetrahedral elements. J. Biomech. 49 (5), 659–667. http://dx.doi.org/10.1016/j.jbiomech.2016.01.024.

Meng, Q., An, S., Damion, R.A., Jin, Z., Wilcox, R., Fisher, J., Jones, A., 2017. The effect of collagen fibril orientation on the biphasic mechanics of articular cartilage. J. Mech. Behav. Biomed. Mater. 65, 439–453. http://dx.doi.org/10.1016/j.jmbbm.2016.09.001.

Ng, K.G., Lamontagne, M., Labrosse, M., Beaulé, P.E., 2016. Hip joint stresses due to cam-type femoroacetabular impingement: a systematic review of finite element simulations. PLoS One 11 (1), e0147813. http://dx.doi.org/10.1371/journal.pone.0147813.

Osawa, T., Moriyama, S., Tanaka, M., 2014. Finite element analysis of hip joint cartilage reproduced from real bone surface geometry based on 3D-CT image. J. Biomed. Sci. Eng. 9 (2), 13-00164. http://dx.doi.org/10.1299/jbse.13-00164.

Petersen, W., Petersen, F., Tillmann, B., 2003. Structure and vascularization of the acetabular labrum with regard to the pathogenesis and healing of labral lesions. Arch. Orthop. Trauma Surg. 123 (6), 283–288. http://dx.doi.org/10.1007/s00402-003-0527-7.

Pfirrmann, C.W., Mengiardi, B., Dora, C., Kalberer, F., Zanetti, M., Hodler, J., 2006. Cam and pincer femoroacetabular impingement: characteristic MR arthrographic findings in 50 patients. Radiology 240 (3), 778–785. http://dx.doi.org/10.1148/radiol.2403050767.

Schindelin, J., Arganda-Carreras, I., Frise, E., Kaynig, V., Longair, M., Pietzsch, T., Preibisch, S., Rueden, C., Saalfeld, S., Schmid, B., Tinevez, J.Y., 2012. Fiji: an open-source platform for biological-image analysis. Nat. Methods 9 (7), 676–682. http://dx.doi.org/10.1038/nmeth.2019.

Sophia Fox, A.J., Bedi, A., Rodeo, S.A., 2009. The basic science of articular cartilage: structure, composition, and function. J. Sport Health Sci. 1 (6), 461–468. http://dx.doi.org/10.1177/1941738109350438.

Tannast, M., Siebenrock, K.A., Anderson, S.E., 2007. Femoroacetabular impingement: radiographic diagnosis—what the radiologist should know. Am. J. Roentgenol. 188 (6), 1540–1552. http://dx.doi.org/10.2214/AJR.06.0921.

Thelen, T., Thelen, P., Demezon, H., Aunoble, S., Le Huec, J.C., 2017. Normative 3D acetabular orientation measurements by the low-dose EOS imaging system in 102 asymptomatic subjects in standing position: analyses by side, gender, pelvic incidence and reproducibility. Orthop. Traumatol. Surg. Res. 103 (2), 209–215. http://dx.doi.org/10.1016/j.otsr.2016.11.010.

Urquhart, N., Philippon, M., Ye, J.E., Simunovic, N., Ayeni, O.R., 2014. Alpha angle correction in femoroacetabular impingement. Knee Surg. Sports Traumatol. Arthrosc. 22 (4), 812–821. http://dx.doi.org/10.1007/s00167-013-2678-6.